

Dear Editor,

We have issued a point-by-point reply to all of the reviewers' comments in the open discussion on the geoscientific-model-development website. This also includes all of the changes made to the manuscript with respect to the comments.

Additionally, we have made some minor editorial changes to the manuscript (tracked in the manuscript) and minor enhancements to the model. A new release of the model has been uploaded to Github and has been assigned a Zenodo DOI (<http://doi.org/10.5281/zenodo.1035878>). The list of changes to the model are as follows:

Improvements:

- Conductivity in the energy equation is the geometric mean of fluid and rock conductivities.
- Result plotting during playback is significantly faster.
- Added an example of an igneous intrusion in a cooled pluton (i.e. no sedimentation or basin evolution involved).

Bug Fixes:

- Fixed plotting issue where in some cases whole range of observed data may not be plotted.
- Time step for last point in youngest sedimentary layer corrected.
- Fixed code so that file separators for Mac and Linux systems are recognized and used.

Best Regards,

Karthik Iyer

Author's Response

Dear Reviewer #1,

Thank you for your constructive review which helped us better evaluate the presented model and make suitable changes where required. A point-by-point answer to the review is as follows (line numbering according to revised manuscript):

1. Please further highlight the novelty of SiLLi by comparing it with some other similar simulators such as MagmaHeatNS1D. MagmaHeatNS1D was developed based on almost the same models and written using an object-oriented language. In comparison, the Silli indeed considers some additional geological processes. Iyer et al. needs to introduce the significance of these processes.

Wang D., MagmaHeatNS1D: One-dimensional visualization numerical simulator for computing thermal evolution in a contact metamorphic aureole, *Computers & Geosciences*, 2013, 54(4): 21-27.

- We have added the reference to Wang, 2013 in the introduction (Line 67) and also further highlighted the uniqueness of SiLLi and the motivation behind the model (Lines 84-93: “The motivation behind the model and manuscript is to make a standardized numerical toolkit openly available that can be widely used by scientists with varying backgrounds to test the effect of magmatic bodies in a wide variety of settings using readily available data such as standard well logs and field measurements. The model incorporates relevant processes associated with heat transfer from magmatic intrusions such as latent heat effects, decarbonation reactions and organic matter maturation and also accounts for background maturation and erosion by systematically reconstructing the entire present-day sedimentary column from the input data. Lastly, the model results can be easily compared to the two most widely used aureole proxies in sedimentary rocks, vitrinite reflectance (VR) and total organic carbon (TOC) data”).
2. Line 153: modeling results are highly sensitive to boundary conditions. What kind of boundary condition is assumed for the upper and lower boundaries by SiLLi? Besides, how to prove that “5 times the thickness of the bottommost sill” is reasonable? Such assumption needs to be made based on either special sensitivity analysis or the results of some similar researches.
- The implementation of temperature boundary conditions to the upper and lower boundaries are already mentioned in Lines 179 to 181 (“The thermal solver computes the temperature within the deposited sedimentary column by applying fixed temperatures at the top and bottom at every step which are calculated from the prescribed geotherm”). We have added the reason and reference to justify that aureole processes are usually limited to less than 400% of sill thickness (Lines 173 to 176: “Note that the bottom boundary is extended to 5 times the thickness of the bottommost sill if that sill is close to or at the bottom boundary (hypothetical basement) in order to remove boundary effects and resolve aureole processes that are mostly limited to less than 4 times the sill thickness (Aarnes et al., 2010).”).
3. Section 3.6: Iyer et al. consider some potential heat sink/source but ignored water boiling and vaporization. Why? For the one-dimensional thermal models, Jeager (1959), Barker et al. (1998, *international journal of coal geology*) Wang et al. (2007, *GRL*) and Wang (2011, *international journal of coal geology*) pointed out its effects on thermal evolution of host rocks. This may be explained in this section.
- A full two-phase flow model would be required to fully capture the effect of pore water boiling and subsequent condensation away from the heat source (e.g. Coumou et al., 2008. Phase separation, brine formation, and salinity variation at Black Smoker hydrothermal systems, *JGR-Solid Earth*). Moreover, previous studies have shown that model effects of the uncertainty of pre water volatilization is as large as the effects of variation in material properties such as heat capacity (Wang 2012. Comparable study on the effect of errors and uncertainties of heat transfer models on quantitative evaluation of thermal alteration in

contact metamorphic aureoles: Thermophysical parameters, intrusion mechanism, pore-water volatilization and mathematical equations). Therefore, we have not implemented pore water volatilization in SILLi as it only adds to further uncertainty in an unconstrained variable.

4. Section 3.6: although most organic-rich rocks are less permeable, Jaeger (1959), Galushkin (1997), Wang and Manga (2015) indeed showed the possible heat convection mechanism in shallowly buried shale host rocks. These work need to cited in this section.
 - The authors acknowledge that in some cases the effect of hydrothermal activity may indeed need to be considered in order to match field data as mentioned by the references above. The use of the Nusselt number approach (enhanced thermal conductivity) for such cases has been outlined in the manuscript (Lines 270 to 276: “Nevertheless, in some cases the effects of hydrothermal activity may be visible where the thermal aureole is larger above than below the sill and is recorded by vitrinite reflectance data (Galushkin, 1997; Wang and Manga, 2015). In such cases, the user may use an enhanced thermal conductivity (up to 5 times the usual rock conductivity) in the layer above the sill following the Nusselt number approach to account for hydrothermal activity and match field data. Note that care should be taken to check if the same effect can also be attributed to changes in other material properties or geological processes.”).

Dear Reviewer #2,

Thank you for your constructive review which helped us better evaluate the presented model and make suitable changes where required. A point-by-point answer to the review is as follows (line numbering according to revised manuscript):

1. A little background and context to the modelling around intrusions would help the reader to see more clearly the novel aspects of this model (for example, perhaps some broader discussion early on as to the wider affects of intrusions on organic rich sedimentary successions, particularly with respect to hydrocarbon prospectivity (although not the primary focus of this paper will certainly be of significant interest to the field and indeed requires some finer background detail in line with the time spent on thermogenic gas, PETM etc). Suggested Refs to broaden background: Archer et al (2005); Rodriguez et al (2005, 2006) – especially for comparison with the 2D models within, alongside some comparison of other modelling methods in refs already noted. Perhaps also Schofield et al 2015 or Muirhead et al 2017 for a broader view on organic matter alteration adjacent to intrusions). Specifically, why is this modelling method more applicable than/or add to the other modelling?
 - We have enhanced the introduction on modelling of sill intrusions by adding a short segment on the effects of intrusives on hydrocarbon prospectivity as suggested with the relevant references (Lines 52-59: “Magmatic intrusions are also of particular interest for hydrocarbon prospectivity and can impact petroleum systems in positive and negative ways (Archer et al., 2005; Monreal et al., 2009; Peace et al., 2017). High temperatures in the thermal aureole

around such intrusions may induce maturation and hydrocarbon generation in immature, shallow strata that may have not been productive under normal burial. On the other hand, pre-emptive maturation of hydrocarbons around an intrusion may result in loss of hydrocarbons if a suitable reservoir has not yet formed. Additionally, pre-existing oil in a reservoir may crack to gas in the vicinity of magmatic intrusions resulting in degradation of a potential prospect.”). We have also modified the introduction so that it better conveys the motivation behind the model and its strengths (Lines 84-93: “The motivation behind the model and manuscript is to make a standardized numerical toolkit openly available that can be widely used by scientists with varying backgrounds to test the effect of magmatic bodies in a wide variety of settings using readily available data such as standard well logs and field measurements. The model incorporates relevant processes associated with heat transfer from magmatic intrusions such as latent heat effects, decarbonation reactions and organic matter maturation and also accounts for background maturation and erosion by systematically reconstructing the entire present-day sedimentary column from the input data. Lastly, the model results can be easily compared to the two most widely used aureole proxies in sedimentary rocks, vitrinite reflectance (VR) and total organic carbon (TOC) data.”).

2. The correlation of modelled and actual TOC and VR is compelling, however the manuscript would benefit from some more detail about how the data is refined e.g. lines 384-386 and how this ties back to the methods above. Although TOC and VR have been typically used as a measurement around sills for decades – how does this correlate to other maturity parameters such as mineralogical markers, biomarkers?
 - We have elaborated on how we refine the input TOC data in the manuscript if this data is not known (Lines 424-429: “Initial average TOC data for the sedimentary layers away from the sill intrusion is not known but can be roughly estimated using present-day values, i.e. the TOC values will be higher than current values as TOC is thermally broken down close to the intrusion. The initial input TOC data is subsequently refined so that a better match of the model results to the observed data is obtained, thereby highlighting how the model can be used to constrain initial conditions within the sedimentary column (Figure 9).”). In order to do so, we first estimate the TOC content, if it is not measured, by using a higher than present day value since TOC is thermally broken down with time. If the values do not result in a good fit to present-day TOC values than the initial input values are subsequently refined until a good fit is obtained. We have also stated that the user can correlate other, ‘non-standard’ maturity parameters themselves using its correlation to the temperature-time evolution from the model results if this correlation is known (Lines 280-282: “Similarly, correlation to other maturity parameters such as mineralogical markers or biomarkers (e.g. Muirhead et al. (2017)) can be performed by the user using the time-temperature evolution from the model if so desired.”).
3. The extent of the thermal aureoles of sills can be measured using TOC and VR (as discussed, among many other parameters). In the Model Input section these are displayed as ‘optional’. Organic matter will frequently thermally alter in very different manners to mineralogical material

and surely one or other parameter must be used to help gauge the full thermal impact of the sill?
Clarity over the use of VR and/or TOC would help the reader.

- Present-day measured TOC and VR values are 'optional' in terms of user-input to the model since these values are not always measured or available. This does not inhibit the user from running the model.

1 **SILLi 1.0: A 1D Numerical Tool Quantifying the Thermal Effects of Sill**
2 **Intrusions**

3 *Karthik Iyer^{1,2}, Henrik Svensen³ and Daniel W. Schmid^{1,4}

4 *karthik.iyer@geomodsol.com

5 1 GeoModelling Solutions GmbH, Zurich, Switzerland

6 2 GEOMAR, Helmholtz Centre for Ocean Research, Kiel, Germany

7 3 Centre for Earth Evolution and Dynamics, University of Oslo, Norway

8 4 Physics of Geological Processes, University of Oslo, Norway

9

10 **Abstract**

11 Igneous intrusions in sedimentary basins may have a profound effect on the thermal structure and
12 physical properties of the hosting sedimentary rocks. These include mechanical effects such as
13 deformation and uplift of sedimentary layers, generation of overpressure, mineral reactions and
14 porosity evolution, and fracturing and vent formation following devolatilization reactions and the
15 generation of CO₂ and CH₄. The gas generation and subsequent migration and venting may have
16 contributed to several of the past climatic changes such as the end-Permian event and the Paleocene-
17 Eocene Thermal Maximum. Additionally, the generation and expulsion of hydrocarbons and cracking of
18 pre-existing oil reservoirs around a hot magmatic intrusion is of significant interest to the energy
19 industry. In this paper, we present a user-friendly 1D FEM based tool, SILLi, which calculates the thermal
20 effects of sill intrusions on the enclosing sedimentary stratigraphy. The model is accompanied by three
21 case studies of sills emplaced in two different sedimentary basins, the Karoo Basin in South Africa and
22 the Vøring Basin offshore Norway. Input data for the model is the present-day well log or sedimentary
23 column with an Excel input file and includes rock parameters such as thermal conductivity, total organic
24 carbon (TOC) content, porosity, and latent heats. The model accounts for sedimentation and burial
25 based on a rate calculated by the sedimentary layer thickness and age. Erosion of the sedimentary
26 column is also included to account for realistic basin evolution. Multiple sills can be emplaced within the
27 system with varying ages. The emplacement of a sill occurs instantaneously. The model can be applied

28 to volcanic sedimentary basins occurring globally. The model output includes the thermal evolution of
29 the sedimentary column through time, and the changes that take place following sill emplacement such
30 as TOC changes, thermal maturity, and the amount of organic and carbonate-derived CO₂. The TOC and
31 vitrinite results can be readily benchmarked within the tool to present-day values measured within the
32 sedimentary column. This allows the user to determine the conditions required to obtain results that
33 match observables and leads to a better understanding of metamorphic processes in sedimentary
34 basins.

35

36 **1 Introduction**

37 Volcanic processes can strongly influence the development of sedimentary basins associated with
38 continental margins. Magmatic bodies such as dikes and sills have a major impact on the thermal
39 evolution of these sedimentary basins. The short-term effects of igneous intrusions include deformation
40 and uplift of the intruded sediments, heating of the host rock, mineral reactions, generation of
41 petroleum, boiling of pore fluids and possible hydrothermal venting (Jamtveit et al., 2004; Malthe-
42 Sorensen et al., 2004; Svensen et al., 2004; Wang et al., 2012b). Long-term effects include focused fluid
43 flow, migration of hydrothermal and petroleum products, formation of mechanically strong dolerite and
44 hornfels in the contact aureole and differential compaction (Iyer et al., 2013; Iyer et al., 2017; Kjoberg et
45 al., 2017; Planke et al., 2005). This is of particular importance to understanding the carbon cycle, as
46 thermal stresses, besides those associated with burial, encountered by organic matter in immature
47 source rocks will determine the ultimate production and fate of the CO₂ and CH₄ generated. Vent
48 structures are intimately associated with sill intrusions in sedimentary basins globally and are thought to
49 have been formed contemporaneously due to overpressure generated by pore-fluid boiling gas
50 generation during thermogenic breakdown of kerogen (Aarnes et al., 2015; Iyer et al., 2017; Jamtveit et
51 al., 2004). Methane and other gases generated during this process may have driven catastrophic climate
52 change in the geological past (Svensen and Jamtveit, 2010; Svensen et al., 2009). Magmatic intrusions
53 are also of particular interest for hydrocarbon prospectivity and can impact petroleum systems in
54 positive and negative ways (Archer et al., 2005; Monreal et al., 2009; Peace et al., 2017). High
55 temperatures in the thermal aureole around such intrusions may induce maturation and hydrocarbon
56 generation in immature, shallow strata that may have not been productive under normal burial. On the
57 other hand, pre-emptive maturation of hydrocarbons around an intrusion may result in loss of
58 hydrocarbons if a suitable reservoir has not yet formed. Additionally, pre-existing oil in a reservoir may

59 [crack to gas in the vicinity of magmatic intrusions resulting in degradation of a potential prospect.](#) -In
60 order to understand these problems, numerical models are widely used to reconstruct the thermal
61 history of a basin where only a few of these parameters are known.

62 A number of analytical and numerical models have been developed that study the thermal effects of
63 igneous intrusions dating back to the early- and mid-1900's (Jaeger, 1964; Jaeger, 1957, 1959; Lovering,
64 1935). Subsequent 1D and 2D models added additional complexity to the models by the addition of
65 emplacement mechanisms and timing, source rock maturation, hydrocarbon generation, latent heats of
66 devolatilization and maturation, fluid processes and overpressure generation (Aarnes et al., 2011a;
67 Fjeldskaar et al., 2008; Galushkin, 1997; Iyer et al., 2017; Monreal et al., 2009; Wang, 2013; Wang, 2012;
68 Wang et al., 2010; Wang and Song, 2012; Wang et al., 2012a). Contact metamorphic processes are well
69 understood (e.g. (Aarnes et al., 2010; Jamtveit et al., 1992; Tracy and Frost, 1991)), but many published
70 papers do not take into account the basin history or the variations in contact aureole thickness that arise
71 from the type of measuring method that has been used. In general, the contact metamorphic effects
72 depend on 1) sill thickness (note that dikes cannot be directly compared with sills), 2) sill emplacement
73 temperature, 3) thermal gradient and emplacement depth (i.e. temperature and background
74 maturation), 4) emplacement history (instantaneous versus prolonged magma flow), 5) host rock
75 composition and characteristics (such as thermal conductivity, organic carbon content, porosity,
76 permeability) and 6) conductive versus advective cooling (e.g. (Aarnes et al., 2010; Galushkin, 1997; Iyer
77 et al., 2013; Iyer et al., 2017; Jaeger, 1964; Lovering, 1935; Wang, 2012)). In addition, the contact
78 aureole width depends on how aureoles are studied and measured. The aureole thickness depends on
79 the proxy used, including sonic velocity, density, mineralogy and mineral properties, magnetic
80 susceptibility, total organic carbon content, vitrinite reflectivity, color, porosity, or organic geochemistry.
81 Note that these aureole thickness proxies will not necessarily give the same result. Finally, the aureole
82 thickness also depends on the proximity to other sills emplaced at the same time (see Aarnes et al.
83 (2011b) for a quantification).

84 In this paper we present a generic 1D thermal model, SILLi, which can be applied to studying the thermal
85 effects of sill intrusions in sedimentary basins globally. [The motivation behind the model and manuscript](#)
86 [is to make a standardized numerical toolkit openly available that can be widely used by scientists with](#)
87 [varying backgrounds to test the effect of magmatic bodies in a wide variety of settings using readily](#)
88 [available data such as standard well logs and field measurements.](#) ~~Besides heat transfer, the model also~~
89 ~~accounts for the sequential deposition of sedimentary layers through time, erosion, latent heat effects~~

90 ~~and gas generation by decarbonation reactions and organic matter maturation. The model incorporates~~
91 ~~relevant processes associated with heat transfer from magmatic intrusions such as latent heat effects,~~
92 ~~decarbonation reactions and organic matter maturation and also accounts for background maturation~~
93 ~~and erosion by systematically reconstructing the entire present-day sedimentary column from the input~~
94 ~~data. Lastly, the model results can be then~~ easily compared to the two most widely used aureole
95 proxies in sedimentary rocks, vitrinite reflectance (VR) and total organic carbon (TOC) data.

96

97 **2 Model Input**

98 The one dimensional, Finite Element Method (FEM) model numerically recreates the thermal effects of
99 sill emplacement in a sedimentary column. The model is written using MATLAB and requires version
100 2014b or higher to run. The model input is specified in an Excel (*.xls) file and is read by the Matlab file,
101 SILLi.m. The user also specifies the model resolution with the igneous intrusions and sedimentary layers
102 by giving the minimum spacing (m) or the minimum number of points in the Matlab file. The measure
103 that produces the highest resolution is used. The Excel file is composed of seven tabs outlined below. If
104 a previously calculated output file is available for the input file, the program prompts the user to choose
105 between loading the output file for further analysis and performing a new calculation which overwrites
106 the existing file.

107 For correct model use, the geological input needs to be based on either a borehole (with horizontal
108 stratigraphy) or an outcrop that is converted into a pseudo-borehole. If the case study is outcrop-based,
109 a pseudo-borehole stratigraphy should be constructed including the regional basin stratigraphy. Note
110 that sedimentary rocks present at higher stratigraphic levels elsewhere in the basin should be added to
111 the erosion history of the basin. Moreover, the sills (and samples) should be rotated back to horizontal if
112 the stratigraphy was tilted post sill emplacement. Using TOC and VR data from sedimentary rocks
113 outside the immediate contact aureoles will improve the model calibration.

114

115 **2.1 Fluid**

116 This tab contains ~~three-four~~ columns describing the fluid name, its density (kg/m^3), ~~and its~~ heat capacity
117 (J/kg/K) and thermal conductivity (W/m/K).

118

119 2.2 Lithology

120 This tab contains the data required for the model to build the present-day sedimentary column. The
121 various columns detail the name of the sedimentary layer (character only) and various material
122 properties such as density (kg/m^3), heat capacity (J/kg/K), porosity (fraction), thermal conductivity
123 (W/m/K), initial TOC content (wt%) and latent heats of organic maturation and dehydration (kJ/kg).
124 Information regarding the kind of carbonate contained in the sedimentary layer can be given in the last
125 column if decarbonation reactions are considered. The mineral constitution of the carbonate can be
126 chosen as marl (1), dolomite (2) or dolomite/evaporite mix (3). A zero (0) is entered in this column if
127 decarbonation reactions are not required. The lithology tab also contains columns where the present-
128 day top depth (m) and age (Ma) of each layer can be given which determine the depositional sequence
129 and sedimentation rate for the layer (see Section 3.1). Note that the ages of the sedimentary must be
130 unique. A hypothetical basement is added 10 m below the deepest sedimentary layer top depth ~~or 300~~
131 ~~m below the bottom of the deepest sill intrusion, whichever is deeper.~~

132

133 2.3 Erosion

134 This tab is similar to the lithology tab and contains information on eroded layers. Additional columns in
135 this tab contain information regarding the erosion timing (Ma) and the thickness of the eroded layer
136 (m). Note that the top depth of the eroded layer must coincide with the top of a sedimentary layer in
137 the lithology tab. If part of sedimentary layer is indeed eroded before deposition continues (i.e. the
138 eroded layer lay inside a deposited layer), the layer needs to be considered as unique layers separated
139 by the eroded layer. Multiple eroded layers can have the same top depths provided that older layers
140 with the same top depth are eroded first. Similarly, eroded layers have to be eroded first prior to
141 deposition of younger layers. The ages of the eroded layers cannot coincide with other layers.

142

143 2.4 Sills

144 This tab contains information necessary for the emplacement of sill intrusions. The top depth (m) and
145 thickness (m) of the sill constrain the geometry of the intrusion. Additional information includes the
146 time of emplacement (Ma), emplacement temperature ($^{\circ}\text{C}$), melt and solid densities (kg/m^3), melt and
147 solid heat capacities (J/kg/K), thermal conductivity (W/m/K), solidus and liquidus temperatures of the
148 magma ($^{\circ}\text{C}$) and the latent heat of crystallization (kJ/kg). The emplacement of the intrusion is assumed

149 to be instantaneous. Note that the top depth of the sill cannot be the same as the top depth of a
150 sedimentary layer. On the same note, the top depth of a sedimentary layer cannot be inside a sill
151 intrusion. Emplacement ages cannot exactly coincide with layer ages.

152

153 **2.5 Temperature Data**

154 This tab contains temperature data (°C) vs. depth (m) for the sedimentary column. The data in this tab is
155 used to construct a geothermal gradient by using the best linear fit and therefore needs to contain at
156 least two data points. Additionally, the first data point must coincide with the column top describing the
157 surface temperature.

158

159 **2.6 Vitrinite Data (Optional)**

160 This tab contains present day vitrinite reflectance data presented in depth (m) and VR values (%Ro).
161 Standard deviation of the values when available can be included. This data is used for comparison of the
162 modelled VR values to observations. This tab can be left blank if no measured information is available.

163

164 **2.7 TOC Data (Optional)**

165 This tab contains present day TOC content data (wt%) vs. depth (m) measured in the sedimentary
166 column which is used to compare to the model results. This tab can be left blank if no measured
167 information is available.

168

169 **3 Method**

170 **3.1 Sediment Deposition and Erosion**

171 Each sedimentary layer, including the eroded layers, is deposited sequentially in time based on the
172 depositional age. The rate of sedimentation for each layer is determined by the thickness of the layer
173 and the difference in time between its top age and that of the layer deposited before it. Erosional layers
174 in the sedimentary column are deposited in the same way as other layers. Erosion of the entire layer
175 occurs within a single step at the specified erosion age. The temperature boundary conditions are

176 accordingly adjusted for the height of the new sedimentary column. Note that the bottom boundary is
 177 extended to 5 times the thickness of the bottommost sill if that sill is close to or at the bottom boundary
 178 (hypothetical basement) in order to remove boundary effects and resolve aureole processes that are
 179 mostly limited to less than 4 times the sill thickness (Aarnes et al., 2010).

180

181 3.2 Thermal Diffusion

182 The thermal solver computes the temperature within the deposited sedimentary column by applying
 183 fixed temperatures at the top and bottom at every step which are calculated from the prescribed
 184 geotherm (see Section 2.5) and the energy diffusion equation,

$$185 \quad \left[\phi \rho_f c_{pf} + (1 - \phi) \rho_r c_{peff} \right] \frac{\partial T}{\partial t} = \nabla \cdot (\kappa_{eff} \nabla T) \quad (1)$$

186 κ_{eff} is the bulk thermal conductivity that includes the rock and fluid contributions as a geometric mean
 187 (Hantschel and Kauerauf, 2009):

$$188 \quad \kappa_{eff} = \kappa_r^{(1-\phi)} \kappa_f^\phi \quad (2)$$

189 Table 1 contains the definitions of all the notations used in the manuscript. The effective rock heat
 190 capacity accounts for the latent heat of fusion in the crystallizing parts of the sill between the solidus (T_S)
 191 and liquidus (T_L) temperature of the magma (e.g. (Galushkin, 1997))

$$192 \quad c_{peff} = c_{pm} \left[1 + \frac{L_c}{(T_L - T_S) c_{pm}} \right] \text{ if } [T_S < T < T_L]$$

$$c_{peff} = c_{pr} \quad \text{ if } [T_S > T]$$

193 Sills are emplaced instantaneously at the specified time and temperature within the sedimentary
 194 column. The emplacement of multiple sills in the same step is possible. The time-steps used for thermal
 195 diffusion after sill emplacement are automatically calculated based on the sill thickness and the
 196 characteristic time required for thermal diffusion. The time step is initially small in order to accurately
 197 resolve the thermal evolution of the contact aureole around the sill and is gradually increased once the
 198 energy released by the cooling sill is dissipated.

Field Code Changed

Field Code Changed

199 Dehydration reactions in the host rock are implemented by modifying the thermal diffusion equation
 200 when temperatures of the sediments increase within a certain range (Galushkin, 1997; Wang, 2012)

$$201 \quad \left[\phi \rho_f c_{pf} + (1 - \phi) \rho_r c_{peff} \right] \frac{\partial T}{\partial t} = \nabla \cdot (\kappa \nabla T) - H \quad (4)$$

$$202 \quad H = \frac{(1 - \phi) \rho_r L_d}{T_{d1} - T_{d2}} \frac{\partial T}{\partial t} \quad (5)$$

Symbol	Description	Units
<i>A</i>	Frequency factor	s ⁻¹
<i>c_{peff}</i>	Effective rock heat capacity	J kg ⁻¹ K ⁻¹
<i>c_{pf}</i>	Fluid heat capacity	J kg ⁻¹ K ⁻¹
<i>c_{pr}</i>	Rock heat capacity	J kg ⁻¹ K ⁻¹
<i>E</i>	Activation energy	KJ mol ⁻¹
<i>f</i>	Stoichiometric factor	
<i>F</i>	Reaction extent	
<i>g</i>	Gravitational acceleration	m s ⁻²
<i>i</i>	Reactive component	
<i>L_c</i>	Latent heat of crystallization	KJ kg ⁻¹
<i>m_{CO₂}</i>	Carbon to CO ₂ conversion factor	3.66
<i>P_{atm}</i>	Atmospheric pressure	10 ⁵ Pa
<i>P_{H₂O}</i>	Hydrostatic pressure	Pa
<i>R_{CO₂}</i>	Rate of CO ₂ generation	kg m ⁻³ s ⁻¹
<i>R_{om}</i>	Rate of organic matter degradation	kg m ⁻³ s ⁻¹
<i>t</i>	Time	s
<i>T_L</i>	Liquidus temperature	°C
<i>T_S</i>	Solidus temperature	°C
<i>T</i>	Temperature	°C
<i>T_{d2} - T_{d1}</i>	Temperature range for dehydration reactions (Galushkin, 1997)	350-650 °C
<i>w</i>	Amount of reactive component	Fraction
<i>Z</i>	Depth	km

ϕ	Rock porosity	Fraction
κ_{eff}	<u>Bulk thermal conductivity</u>	<u>W m⁻¹ K⁻¹</u>
κ_r	<u>Rock thermal conductivity</u>	<u>W m⁻¹ K⁻¹</u>
κ_f	<u>Fluid thermal conductivity</u>	W m ⁻¹ K ⁻¹
ρ_f	Fluid density	kg m ⁻³
ρ_r	Rock density	kg m ⁻³

203 Table 1. Definition of symbols used in the model.

204

205 3.3 Thermal Maturation of Organic Matter

206 Vitrinite reflectance is a widely used indicator of thermal maturity and can be readily measured in the
 207 field. One of the most common methods used to calculate the thermal maturity of the source rock is the
 208 EASY%Ro method put forward by Sweeney and Burnham (1990). This model uses 20 parallel Arrhenius-
 209 type of first order reactions to describe the complex process of kerogen breakdown due to temperature
 210 increase. The reaction for the i^{th} component is given by

$$211 \quad \frac{dw_i}{dt} = -w_i A \exp\left[-\frac{E_i}{RT^t}\right] \quad (6)$$

212 where w_i is the amount of material for component i , E_i is the activation energy for the given reaction and
 213 T^t is time-dependent temperature.

214 The total amount of material reacted is obtained by summing up the individual reactions

$$215 \quad \frac{dw}{dt} = \sum_i \frac{dw_i}{dt} \quad (7)$$

216 The fraction of reactant converted is

$$217 \quad F = 1 - \frac{w}{w_0} = 1 - \sum_i f_i \left(\frac{w_i}{w_{0i}} \right) \quad (8)$$

218 from which the vitrinite reflectance can be readily calculated by

219
$$\%Ro = \exp(-1.6 + 3.7F) \quad (9)$$

220 The amount of TOC that has reacted for any given time can be calculated by

221
$$\text{TOC}(t) = \text{TOC}_o F(t) \quad (10)$$

222 and the rate of organic matter degradation by

223
$$R_{om} = (1 - \phi) \rho_r \frac{\partial \text{TOC}}{\partial t} \quad (11)$$

224 The maximum amount of TOC that can be reacted by this method is 85% of the initial total. Note that in
 225 the inner part of the contact aureole close the sill, data shows that all of the organic matter has been
 226 reacted or removed (eg. LA1/68 in section 5.2.2). We assume that all of the hydrocarbons released
 227 during thermal degradation are converted into carbon dioxide. The amount of organic carbon dioxide
 228 generated (R_{CO_2}) for a time step is given by

229
$$R_{CO_2} = R_{om} m_{CO_2} \quad (12)$$

230 where m_{CO_2} is a stoichiometric conversion factor (3.67) to transform carbon into carbon dioxide. Note
 231 that metamorphism of sedimentary rocks will generate CH_4 (e.g., (Aarnes et al., 2010; Iyer et al., 2017)),
 232 but in our model the reacted carbon is recalculated to CO_2 . If needed, the CO_2 model output can be
 233 easily converted to either C or CH_4 .

234 The latent heat of organic maturation is accounted for in the energy equation

235
$$\left[\phi \rho_f c_{pf} + (1 - \phi) \rho_r c_{peff} \right] \frac{\partial T}{\partial t} = \nabla \cdot (\kappa \nabla T) - H - L_{om} R_{om} \quad (13)$$

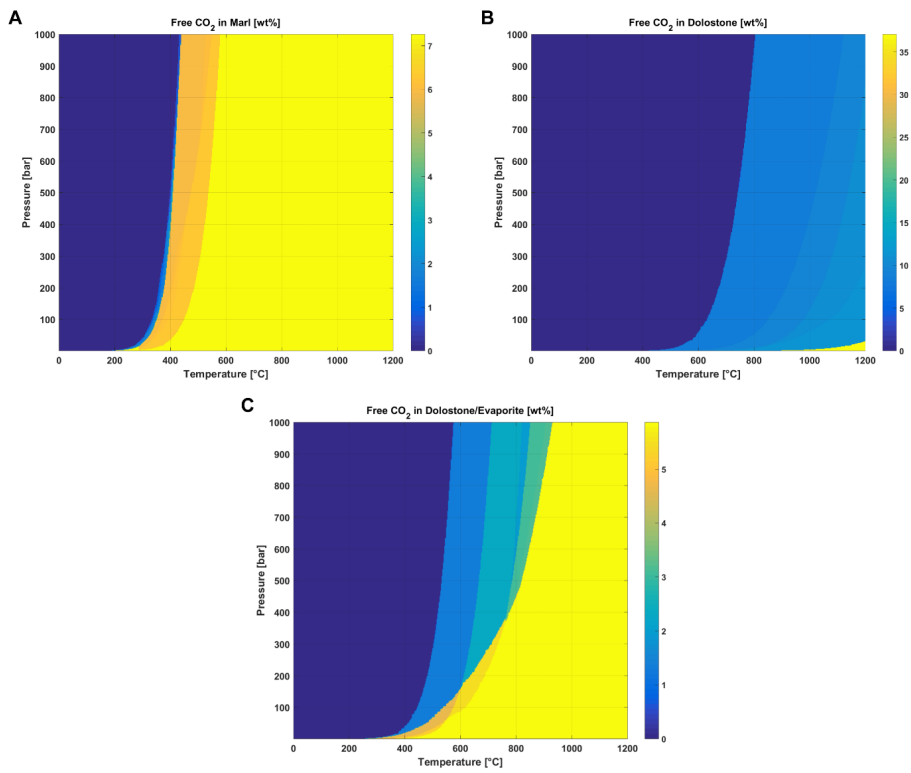
236

237 3.4 Mineral Decarbonation

238 Carbonate minerals undergo decarbonation reactions as they are heated to high temperatures. This
 239 results in mineral transformations and the release of inorganic carbon dioxide which may significantly
 240 add to the CO_2 budget associated with igneous intrusions. The amount of inorganic CO_2 liberated during
 241 metamorphic transformation over a range of temperature and fluid pressure for marl, dolomite and
 242 dolomite/evaporite mixture is pre-computed as a phase diagram using Perple_X (Connolly and Petrini,

243 2002) (Figure 1). The model evaluates the total amount of inorganic CO₂ liberated by carbonate
 244 layers based on the temperature and pressure evolution of the layer through time within the phase
 245 diagrams. Fluid pressure within the sedimentary column is calculated by integrating the rock density
 246 over depth in addition to atmospheric pressure:

247
$$P_{H_2O} = P_{am} + \int_{Z_{min}}^{Z_{max}} \rho_f \bar{g} \quad (14)$$



248
 249 *Figure 1. Phase diagrams generated by Perple_X showing the amounts of inorganic CO₂ liberated with*
 250 *respect to temperature and pressure for marl (A), dolostone (B) and dolostone/evaporite (C).*

251

252 3.5 Model Mesh and Time-Stepping

253 The entire sedimentary column including the eroded layers and igneous intrusions is reconstructed and
254 the column nodes and elements for the FEM model are generated using the user-specified resolution.
255 The nodes are initially collapsed onto each other in depth. Each sedimentary node is assigned a time
256 during which it is expanded (or deposited) within the sedimentary column based on the layer age and its
257 thickness. All of the elements and nodes associated with each igneous intrusion are expanded
258 simultaneously during the corresponding emplacement time. Eroded layers are removed in a single time
259 step specified by the erosion age and the corresponding nodes are collapsed. In order to correctly
260 capture thermal diffusion across the large thermal gradient adjacent to a hot intrusion, the time step is
261 initially very small and exponentially increases during the heating period after sill emplacement and
262 before the next depositional event. The heating period of the sill, over which the exponential time sub-
263 stepping is used, is analytically determined from the characteristic diffusion time for the sill thickness
264 (Jaeger, 1959).

265 3.6 Model Limitations

- 266 • The model is one-dimensional and will therefore not resolve thermal effects that would require
267 a full 3D model.
- 268 • The model does not account for advective transport of heat through the system by fluids.
269 However, previous models have shown that this process would be dominant only in high
270 permeability systems or at the sill edges/tips in low permeability systems (Iyer et al., 2013; Iyer
271 et al., 2017). Therefore, the model presented in this manuscript works well for relatively low
272 permeability systems with shales, mudstone etc. and when the sedimentary column passes
273 through the sill interior away from the edges. Nevertheless, in some cases the effects of
274 hydrothermal activity may be visible where the thermal aureole is larger above than below the
275 sill and is recorded by vitrinite reflectance data (Galushkin, 1997; Wang and Manga, 2015). In
276 such cases, the user may use an enhanced thermal conductivity (up to 5 times the usual rock
277 conductivity) in the layer above the sill following the Nusselt number approach to account for
278 hydrothermal activity and match field data. Note that care should be taken to check if the same
279 effect can also be attributed to changes in other material properties or geological processes.
- 280 • The model does not account for other mineral reactions in the contact aureole besides
281 decarbonation of carbonates. The various mineral reactions possible in the contact aureole can
282 be implemented as an add-on module to the model if needed using the thermal evolution of the

283 [sedimentary column obtained from the model. Similarly, correlation to other maturity](#)
284 [parameters such as mineralogical markers or biomarkers \(e.g. Muirhead et al. \(2017\)\) can be](#)
285 [performed by the user using the time-temperature evolution from the model if so desired.](#)

- 286 • The model assumes that TOC conversion in all types of sedimentary rocks can be estimated by
287 using the EASY%Ro method with a maximum conversion value of 85%. Although, this is a good
288 first approximation, it cannot account for the complete loss of carbon in zones very close to the
289 sill-host rock interface which would result in an underestimation of the released gases (Svensen
290 et al., 2015). On the other hand, the provenance of the sedimentary rock can also significantly
291 affect how kerogen present in organic matter reacts to form hydrocarbons which may result in a
292 reduction in the amount of convertible organic matter due to the presence of inert kerogen (Iyer
293 et al., 2017; Pepper and Corvi, 1995).

295 4 Model Output

296 The model input and results are presented with the help of a GUI (Section 4.6). Model data are written
297 out as a single .mat (Matlab data) file in the same directory as the user-defined path for the input Excel
298 file and with the same filename. The file contains five 'struct' variables of which three contain input
299 information (rock, sill and welldata) and the other two contain model results (result and release). The
300 structure of the variables are described below.

302 4.1 Struct Variable: rock

303 This variable contains input information on the sedimentary layers in the column including the eroded
304 layers. The information is saved as variables given in Table 2 and is sorted according to their top depths.
305 Note that top depths are corrected for the eroded layers that are also included.

<u>Variable Name</u>	<u>Description</u>
Name	User-defined names of all the sedimentary layers in the column.
num	Total number of deposited sedimentary layers.
top	Top depth of the shallowest sedimentary layer.
bot	Top depth of the deepest sedimentary layer.
Tops	Top depths of sedimentary layers.

Ages	Ages of sedimentary layers.
Rho	Density of sedimentary layers.
Cp	Heat capacity of sedimentary layers.
Phi	Porosity of sedimentary layers.
K	Thermal conductivity of sedimentary layers.
Toc	TOC content of sedimentary layers.
Lm	Latent heat of maturation of sedimentary layers.
Ld	Latent heat of dehydration of sedimentary layers.
Carb	Carbonate layer identifier (0-3).
Ero_t	Erosion age of sedimentary layers (NaN if layer is not eroded).
Ero_thick	Eroded thickness of sedimentary layers (NaN if layer is not eroded).
Ero_tops	Top depths of the eroded layers only.

306 *Table 2. List of variables in 'rock' struct variable of the output file.*

307

308 **4.2 Struct Variable: sill**

309 This variable contains input information on sill intrusions in the column. The information is saved as
310 variables given in Table 3 and is sorted according to their top depths.

<u>Variable Name</u>	<u>Description</u>
num	Total number of sill intrusions.
Tops	Top depths of sill intrusions.
E_time	Emplacement ages of sill intrusions.
E_temp	Emplacement temperatures of sill intrusions.
Rhom	Melt density of sill intrusions.
Cpm	Melt heat capacity of sill intrusions.
Rhos	Solid density of sill intrusions.
Cps	Solid heat capacity of sill intrusions.
K	Thermal conductivity of sedimentary layers.
Sol	Solidus of melt in sill intrusions.
Liq	Liquidus of melt in sill intrusions.

Ld	Latent heat of crystallization of melt in sill intrusions.
-----------	--

311 *Table 3. List of variables in 'sill' struct variable of the output file.*

312

313 **4.3 Struct Variable: welldata**

314 This variable contains input information on measured TOC, VR and temperature data for the
315 sedimentary column. The information is saved as variables given in Table 4.

<u>Variable Name</u>	<u>Description</u>
TOC	Measured TOC data vs. depth.
VR	Measured VR data vs. depth.
T	Measured temperature data vs. depth.

316 *Table 4. List of variables in 'welldata' struct variable of the output file.*

317

318 **4.4 Struct Variable: result**

319 This variable contains the model results which are saved for every time step when applicable, i.e.
320 variables that change over time have rows corresponding to the element or node number (depending
321 on where they are defined) and columns corresponding to the time step number. The information is
322 saved as variables given in Table 5.

<u>Variable Name</u>	<u>Description (Rows x Columns)</u>
nel	Number of elements in the model (1 x 1)
nnod	Number of nodes in the model (1 x 1)
Gcoord_c	Depth of element centers (1 x no. of elements)
Ind	Internal nodal indexing of sedimentary layers and intrusions (no. of nodes x 1). Intrusions are negatively indexed.
Ind_nel	Internal element indexing of sedimentary layers and intrusions (no. of elements x 1). Intrusions are negatively indexed.
Ind_carb	Nodal indexing of carbonate layers (0-3) (no. of nodes x 1).
Gcoord	Depth of nodes (no. of nodes x no. of time steps).
Temp	Nodal temperature (no. of nodes x no. of time steps).

Pres	Nodal hydrostatic pressure (no. of nodes x no. of time steps).
Toc	Remaining Toc content at nodes (no. of nodes x no. of time steps).
CO2_org	Organic carbon dioxide generated at nodes (no. of nodes x no. of time steps).
Ro	VR at nodes (no. of nodes x no. of time steps).
Tmax	Maximum temperature experienced at nodes (no. of nodes x no. of time steps).
Active	Binary index of 'deposited/expanded' nodes (no. of nodes x no. of time steps).
CO2_release	Inorganic carbon dioxide generated at nodes (no. of nodes x no. of time steps).
Time	Year count for time step (no. of time steps x 1).

323 Table 5. List of variables in 'result' struct variable of the output file.

324

325 4.5 Struct Variable: release

326 This variable contains the amounts of CO₂ released for every time step normalized to rock volume. The
 327 information is saved as variables given in Table 6.

<u>Variable Name</u>	<u>Description (Rows x Columns)</u>
CO2_org	Organic carbon dioxide generated in elements normalized to rock volume (no. of elements x no. of time steps).
CO2_rel	Inorganic carbon dioxide generated in elements normalized to rock volume (no. of elements x no. of time steps).

328 Table 6. List of variables in 'release' struct variable of the output file.

329

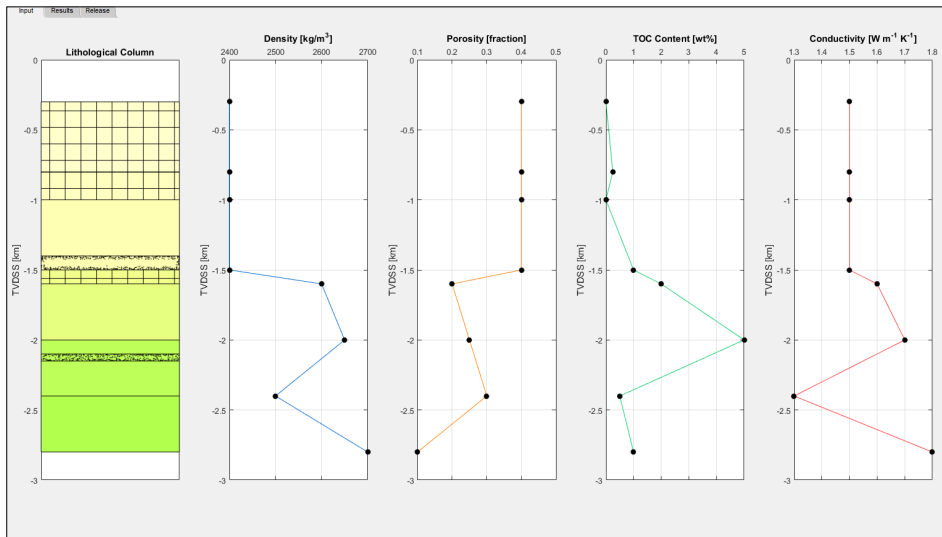
330 4.6 Output Graphical User Interface (GUI)

331 The GUI presented during and after the model run contains three tabs containing graphical
 332 representations of the input data, time evolution of model results and CO₂ release through time. An
 333 explanation of the tabs is given below using a hypothetical test case consisting of a sedimentary column
 334 with two sill intrusions and three eroded layers.

335 4.6.1 Input Tab

336 The left-most subplot of the input tab contains the reconstructed sedimentary column where the layers
 337 are colored according to their depositional age (<http://www.stratigraphy.org/index.php/ics-chart->

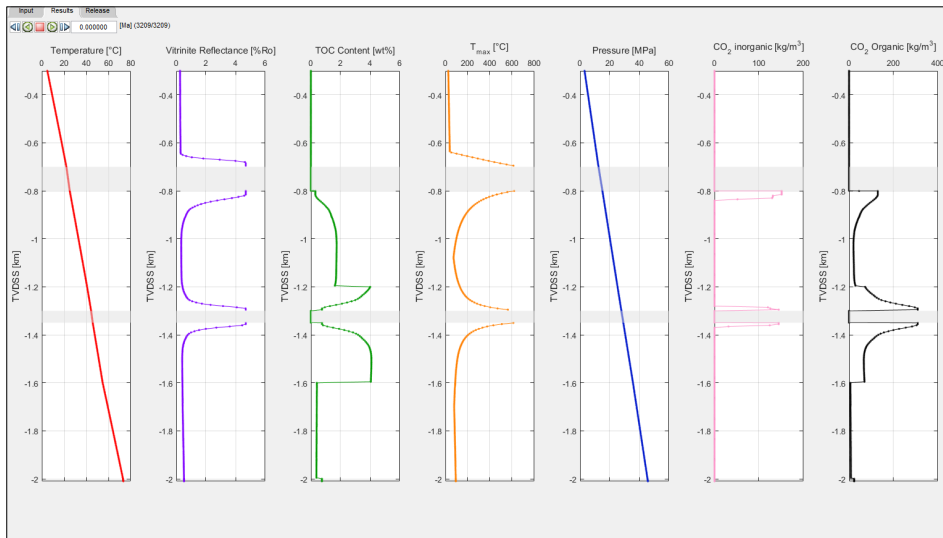
338 [timescale](#)) ([Figure 2](#)). The sedimentary column also contains eroded layers (hatched) and sill
 339 intrusions (speckled). The name and depositional age of a layer can be found by right-clicking the layer.
 340 The other subplots in the input tab contain information on the density, porosity, initial TOC content and
 341 thermal conductivity of the sedimentary layers. The values of these variables are plotted at the
 342 corresponding layer top depth.



343
 344 *Figure 2. Snapshot of the input tab generated for a hypothetical sedimentary column with two sill*
 345 *intrusions and three eroded layers. Right-clicking a layer in the sedimentary column provides the name*
 346 *and depositional/erosional age of the layer.*

347 4.6.2 Results Tab

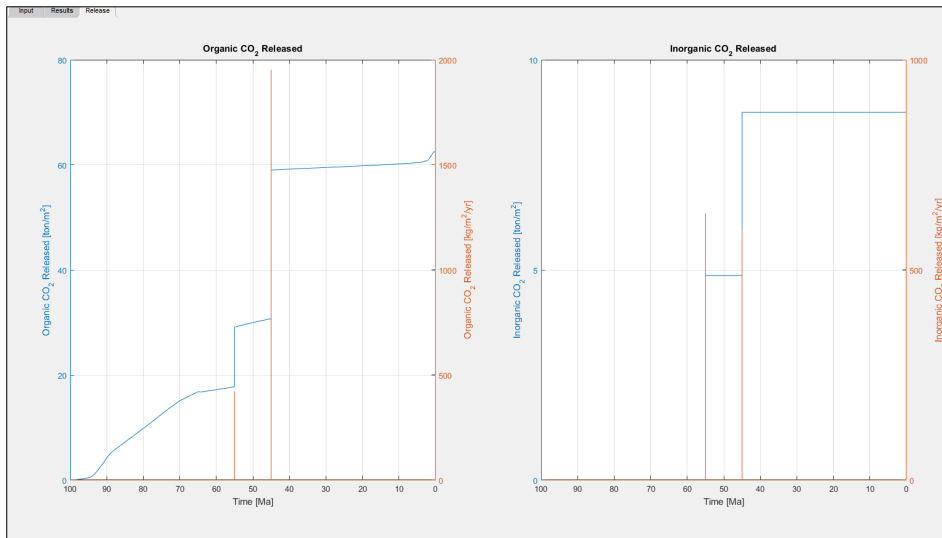
348 The results tab consists of the evolution of temperature, vitrinite reflectance, TOC content, maximum
 349 temperature, hydrostatic pressure, inorganic and organic CO₂ release within the sedimentary column
 350 over simulated time ([Figure 3](#)). The evolution of these variables can be played or stepped
 351 through using the player controls in the top left corner. Alternatively, the user can jump directly to the
 352 desired geological time by inputting it in the player control. Note that this results in the plot jumping to
 353 the time-step nearest the desired time input. Regions containing sill intrusions are highlighted in gray.
 354 Users can copy plot data at any time step by right-clicking the curve.



355
 356 *Figure 3. Snapshot of the results tab generated for a hypothetical sedimentary column with two sill*
 357 *intrusions and three eroded layers. Right-clicking any curve allows the user to copy curve data.*

358 **4.6.3 Release Tab**

359 The release tab plots the cumulative and rates of release of organic and inorganic CO₂ due to heating of
 360 the sedimentary layer by sill intrusions (Figure 4). The cumulative and release rates are summed
 361 over the entire sedimentary column. The user can use the cumulative amount of gas released to easily
 362 upscale to basin scales by multiplying the value by the area affected by sill intrusions. Users can copy
 363 plot data at any time step by right-clicking the curve.



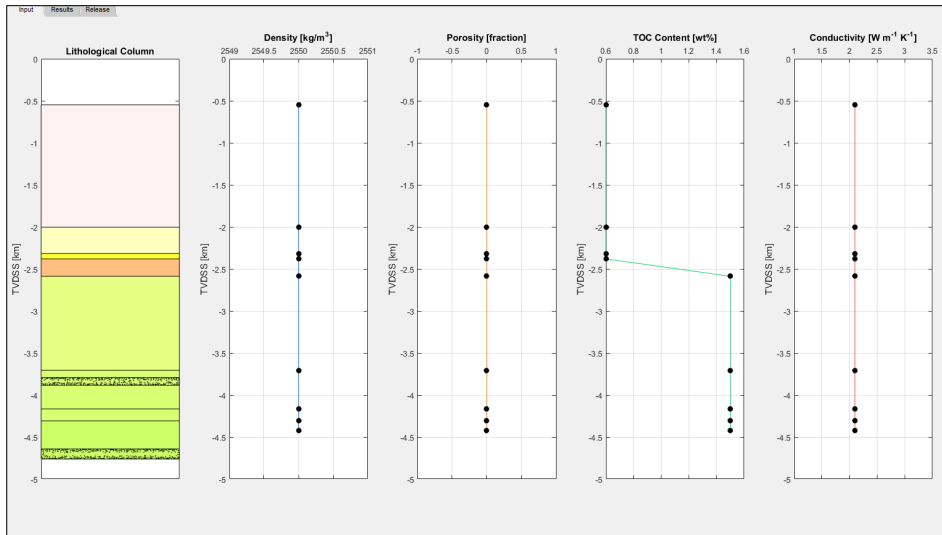
364
 365 *Figure 4. Snapshot of the release tab generated for a hypothetical sedimentary column with two sill*
 366 *intrusions and three eroded layers. Right-clicking any curve allows the user to copy curve data.*

367
 368 **5 Examples**
 369 The examples below are provided with the code and are used to benchmark observations to model
 370 results.

371 **5.1 Utgard High**

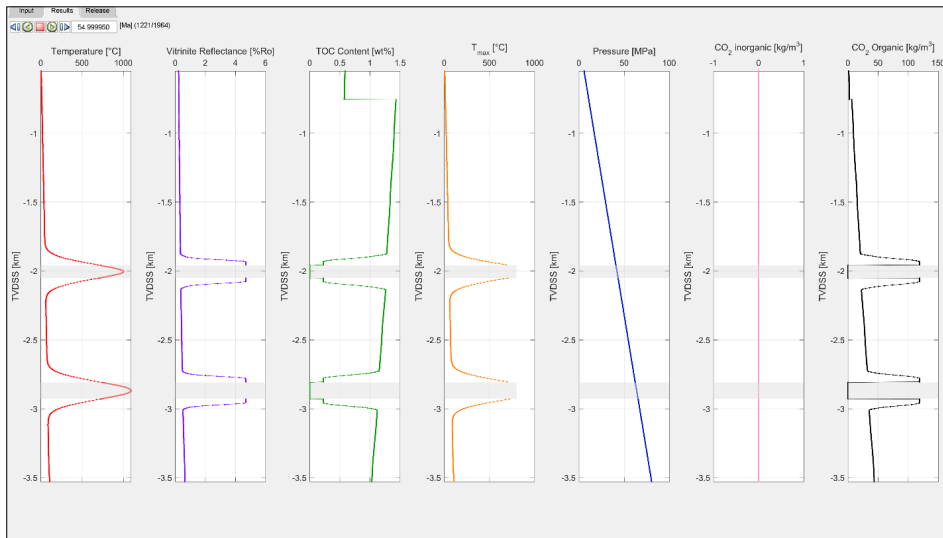
372 The Utgard sill complex is part of the North Atlantic Igneous Province (NAIP) in the Vøring and Møre
 373 Basins, offshore Norway. This region underwent massive volcanic activity at the Paleocene-Eocene
 374 boundary around ~55 Ma (Aarnes et al., 2015). The Utgard High borehole 6607/5-2 was drilled through
 375 two sills emplaced in the Upper Cretaceous sedimentary layers. The drilled lithological column consists
 376 of nine layers with the oldest being deposited 100 Ma (NPD Factpages,
 377 <http://factpages.npd.no/factpages/>) (Figure 5). For simplicity, the material properties of the
 378 entire sedimentary column is set to constant values with the exception of TOC content. TOC content of
 379 the Paleocene and Upper Cretaceous sedimentary layers are set to an initial value of 0.6 and 1.5 wt%,
 380 respectively. Carbonate and erosional layers are not considered. The modelled sedimentary layers are

381 sequentially deposited at the sedimentation rate calculated from the layer top ages. The two sills are
382 emplaced simultaneously within the Nise and Kvitnos Formations at 55 Ma at a temperature of 1150°C.
383 Sedimentary rocks around the emplaced sills are progressively heated as the sills cool. The vitrinite
384 reflectance values increase and the TOC content reduced by thermally degrading organic matter to form
385 CO₂ (Figure 6Figure-6). Sedimentation after sill emplacement results in further burial and extension to
386 produce the present-day sedimentary column. Vitrinite reflectance and TOC data from the Norwegian
387 Petroleum Directorate (NPD) and a previous study (Aarnes et al., 2015) are used to benchmark the
388 model and match very well with the modelled results (Figure 7Figure-7). Further information about the
389 geological and model setting can be found in Aarnes et al. (2015) and the input file
390 '1d_sill_input_utgard.xlsx'.



391

392 Figure 5. Input tab for the Utgard High example.

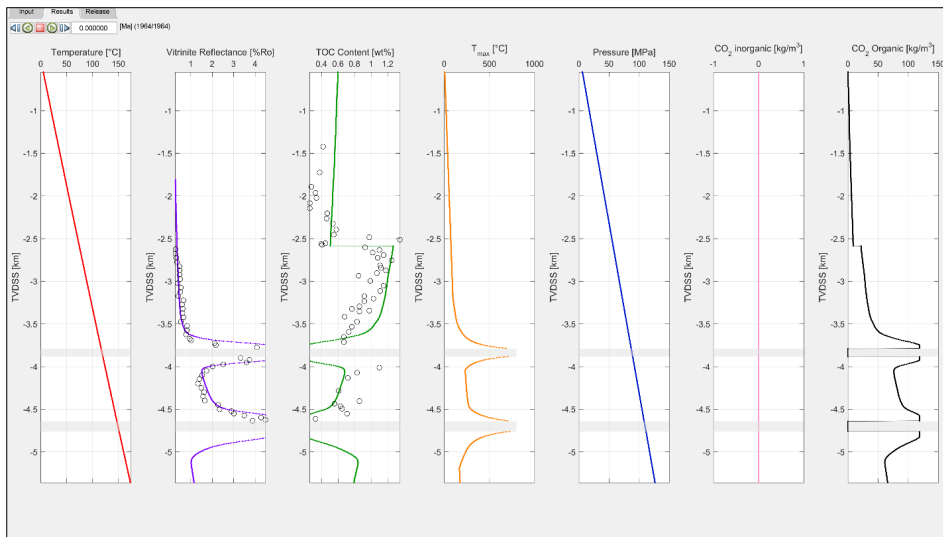


393

394 *Figure 6. Results tab 50 years after the emplacement of sills at 55 Ma for the Utgard High example.*

395 *Sediments around the sills are heated and CO₂ is liberated as organic matter is thermally degraded.*

396



397

398 *Figure 7. Results tab at the end of simulation time for the Utgard High example. The present-day VR and*
399 *TOC values (circles) show a good match with the model results.*

400

401 **5.2 Example 2**

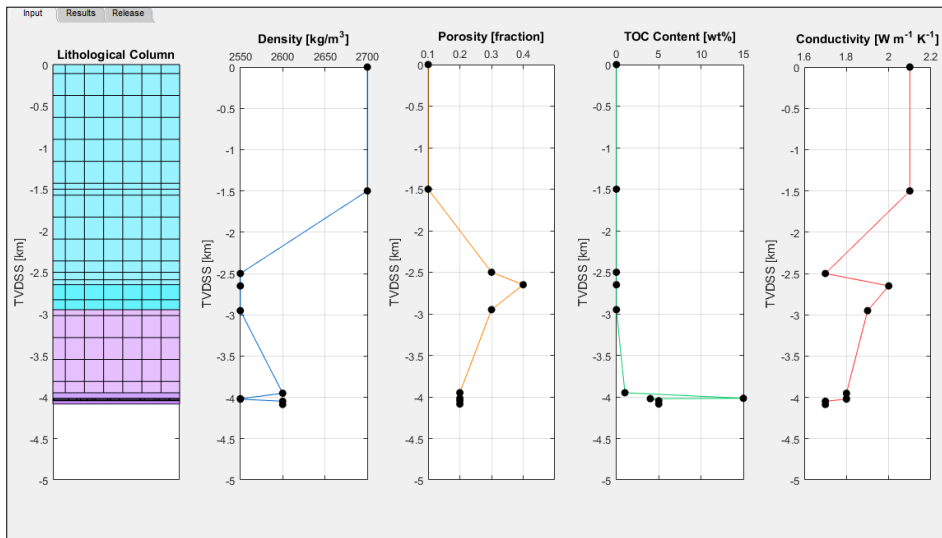
402 The Karoo Large igneous province was emplaced through the Karoo Basin in South Africa in the Early
403 Jurassic. The basin contains sills and dykes of varying thickness (Chevallier and Woodford, 1999; du Toit,
404 1920; Svensen et al., 2015; Walker and Poldervaart, 1949) , emplaced at about 182.6 Ma (Svensen et al.,
405 2012). The basin stratigraphy consists of the Upper Carboniferous to the Triassic Karoo Supergroup and
406 is divided in five groups (the Dwyka, Ecca, Beaufort, Stormberg and Drakensberg groups) with a
407 postulated maximum cumulative thickness of 12 km and a preserved maximum thickness of 5.5 km
408 (Tankard et al., 2009). The depositional environments of the sediments range from marine and glacial
409 (the Dwyka Group), marine to deltaic (the Ecca Group), to fluvial (the Beaufort Group) and finally eolian
410 (the Stormberg Group) (Catuneanu et al., 1998). The Karoo Basin is overlain by 1.65 km of preserved
411 volcanic rocks of the Drakensberg Group, consisting mainly of stacked basalt flows erupted in a
412 continental and dry environment (e.g., (Duncan et al., 1984)). Several recent studies have been devoted
413 to contact metamorphism of the organic-rich Ecca Group (Aarnes et al., 2011b; Moorcroft and
414 Tonnelier, 2016) and the possible consequences of thermogenic methane venting on the Early Jurassic
415 climate (Svensen et al., 2007; Svensen et al., 2015). Here we present two borehole cases from the
416 central (borehole KL1/78) and eastern (borehole LA1/68) parts of the basin previously studied and
417 modelled by Aarnes et al. (2011b) and Svensen et al. (2015), respectively. The details regarding the
418 relative timing of sill emplacement is poorly constrained and we thus use the same age for all sills. If the
419 sills are closely spaced, this will result in a higher maximum temperature in the sedimentary rocks
420 between the sills (cf. (Aarnes et al., 2011b)). For the erosion history of the Karoo Basin, we refer to
421 Braun et al. (2014) and a rapid Late Cretaceous erosion event.

422 **5.2.1 Karoo KL1/78**

423 The first example from the Karoo Basin is a short borehole with a length of 136 m that penetrates the
424 Tierberg, Whitehill and Prince Albert Formations. However, these Formations underlie a massive erosion
425 sequence consisting of 2.5 km of extrusives (Drakensberg Group) and 1.5 km of sediments (Stormberg
426 and Beaufort Groups) and are also included in the model. The borehole penetrates a single 15m thick sill
427 at a depth of 72m ([Figure 8](#)~~Figure 8~~). The sill is emplaced within the Prince Albert Formation at 182.6 Ma

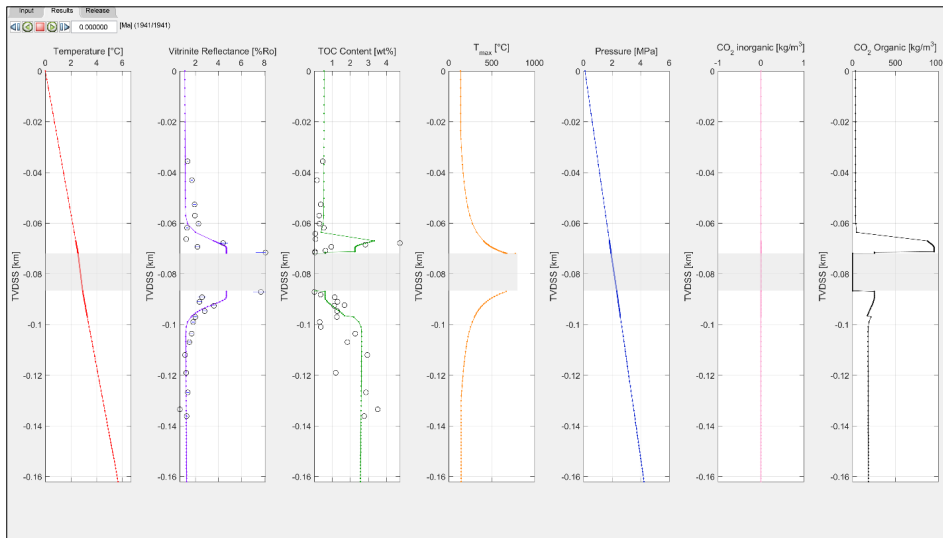
428 at a temperature of 1150°C. Initial average TOC data for the sedimentary layers away from the sill
429 intrusion is not known but can be roughly estimated using present-day values, i.e. the TOC values will be
430 higher than current values as TOC is thermally broken down close to the intrusion. The initial input TOC
431 data is subsequently refined so that a better match of the model results to the observed data is
432 obtained, thereby highlighting how the model can be used to constrain initial conditions within the
433 sedimentary column (Figure 9). The importance of considering the entire basin history when
434 constructing the model is also emphasized by the VR results. The values of the VR results unaffected by
435 the sill would be much lower than the observed values if the eroded sequences are not considered.
436 Addition of these layers to the model results in added burial than would be expected than by just using
437 the 136 m deep borehole. This translates the VR curve laterally thereby better fitting the observed
438 values (Figure 9). The final model shows a good fit of TOC and VR to present day values. Model
439 input data can be found in '1d_sill_input_kl178.xlsx'.

440



441

442 *Figure 8. Input tab for KL1/78.*

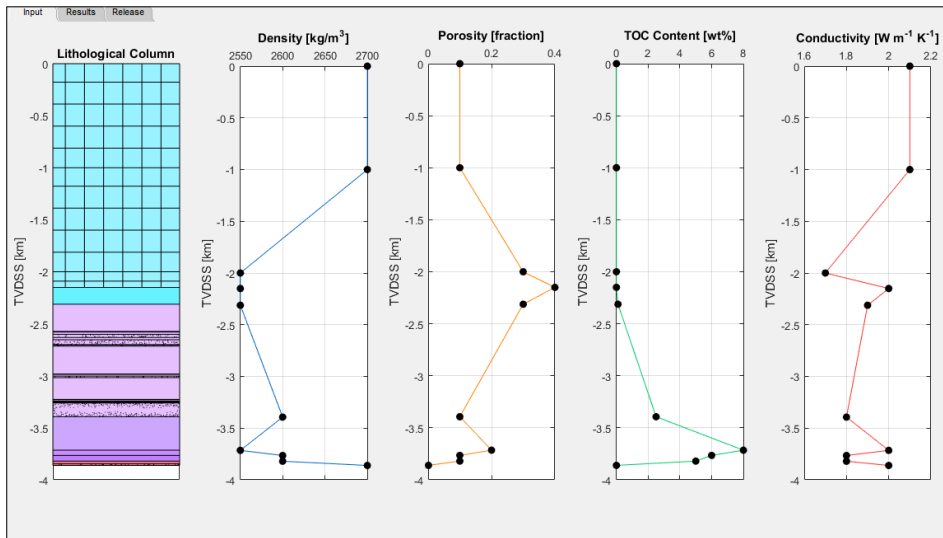


443
 444 *Figure 9. Results tab at the end of simulation time for KL1/78 shows a good match to present-day TOC*
 445 *and VR values.*

446

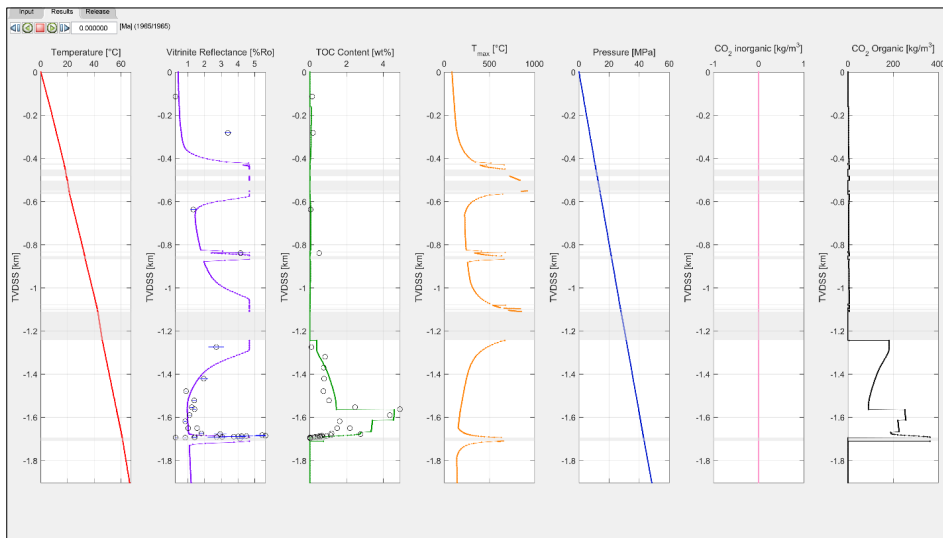
447 **5.2.2 Karoo LA1/68**

448 The second example from the Karoo Basin is a borehole with a length of 1711 m that penetrates the
 449 basin down to the basement (Svensen et al., 2015). Additional erosional sequence consisting mostly of
 450 the Drakensberg lavas and a minor section of the Stormberg Group is also added. The borehole
 451 penetrates multiple sills throughout the entire column with thicknesses ranging from 2 to 132m ([Figure](#)
 452 [10Figure 10](#)). Initial average TOC data for the sedimentary layers is estimated from present-day values.
 453 Similar to the previous example, material properties are iteratively changed within realistic bounds to
 454 arrive at an initial setup that matches the final observations well ([Figure 11Figure 11](#)). Model input data
 455 can be found in '1d_sill_input_la168.xlsx'.



456

457 Figure 10. Input tab for LA1/68.



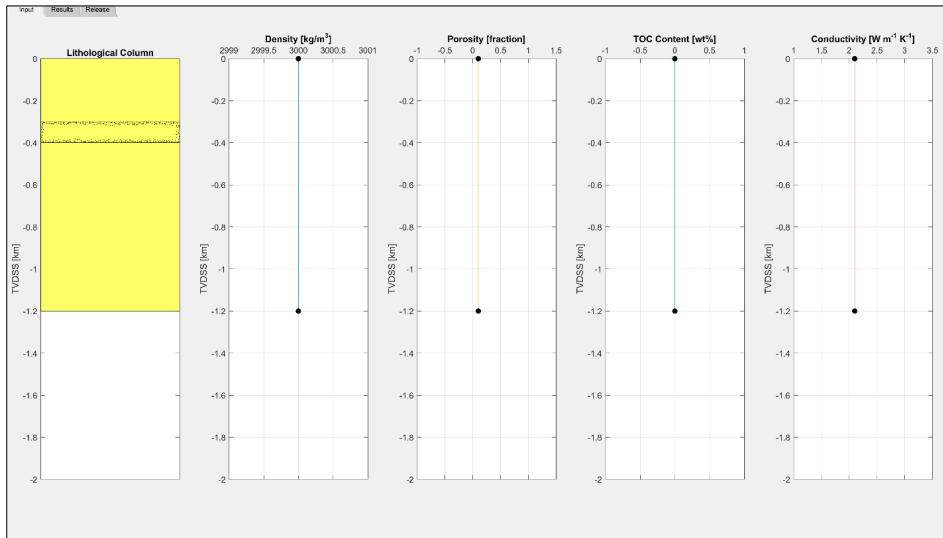
458

459 Figure 11. Results tab at the end of simulation time for LA1/68 shows a good match to present-day TOC
 460 and VR values.

461

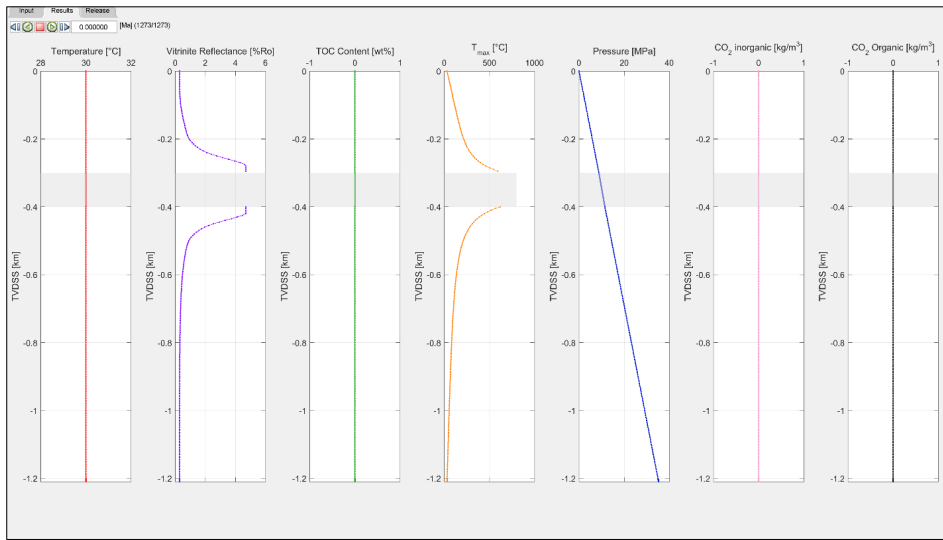
462 **5.3 Intrusion into a Pluton**

463 This example has been added to provide an instance where the user may be interested in modelling the
464 thermal aureole of an emplaced sill or dyke but without the effects associated with deposition of
465 sedimentary layers and the thermal evolution of a basin, e.g. emplacement within an igneous or
466 metamorphic rock. Here, we consider an emplacement of a 100m thick sill into a 1.2km thick igneous
467 body that has cooled to a uniform temperature of 30°C (Figure 12). The host rock is constructed by
468 defining a top and bottom layer with the same material properties and ages that are very close to each
469 other (the code does not allow for two layers with the exact same age). In this example the top and
470 bottom layers have ages of 10 and 10.0001 Ma, respectively, and the intrusion is emplaced at 1 Ma. A
471 constant temperature for the host rock is defined by assigning the same temperature, 30°C, to both
472 intervals in the temperature tab of the excel input file. Thus, the thermal evolution of the intrusion can
473 be investigated independent of burial effects of a sedimentary basin if so desired (Figure 13). Further
474 information about the model setting can be found in the input file '1d_sill_input_dyke.xlsx'.



475

476 Figure 12. Input tab for the Pluton example.



477
 478 *Figure 13. Results tab at the end of simulation time for the pluton example. VR and TOC data are not*
 479 *present for this hypothetical case.*

480

481 **6 Conclusions**

- 482 • SILLi is a numerical model quantifies the thermal evolution of contact aureoles around sills
- 483 emplaced in sedimentary basins. The model includes basin history (burial and erosion), thus
- 484 providing background-maturation levels of organic matter and consequently more realistic gas
- 485 production estimates.
- 486 • SILLi is a user-friendly tool that is written in Matlab and uses Excel for input data.
- 487 • The 1D tool allows for the quick quantification of the thermal effects of sill intrusions. The
- 488 results can be, therefore, used to further constrain and test the initial conditions that may have
- 489 been present within the lithological column that match present-day observations.
- 490 • Model output includes peak temperature profiles, post-metamorphic TOC content, vitrinite
- 491 reflectivity, and the cumulative amount and rate of CO₂ generation. These values can be readily
- 492 upscaled to basin scales if the sill extent is known. The amount of CO₂ can also be easily
- 493 converted to other carbon-bearing gases such as CH₄.

- 494 • Our three case studies demonstrate a good fit between aureole data (TOC and vitrinite
495 reflectivity) and model output showing that the model can be successfully applied to basins in
496 various global settings.

497

498 **7 Code Availability and Software Requirements**

499 The source code with examples is archived as a repository on Github/Zenodo (DOI:
500 <https://doi.org/10.5281/ZENODO.803748> <https://doi.org/10.5281/zenodo.1035878>). Matlab 2014b or
501 higher is required to run the code and Microsoft Excel or any equivalent software is required to edit .xls
502 files.

503

504 **8 License (BSD-2-Clause)**

505 Copyright 2016 Karthik Iyer, Henrik Svensen and Daniel W. Schmid

506 Redistribution and use in source and binary forms, with or without modification, are permitted provided
507 that the following conditions are met:

508 1. Redistributions of source code must retain the above copyright notice, this list of conditions and the
509 following disclaimer.

510 2. Redistributions in binary form must reproduce the above copyright notice, this list of conditions and
511 the following disclaimer in the documentation and/or other materials provided with the distribution.

512 THIS SOFTWARE IS PROVIDED BY THE COPYRIGHT HOLDERS AND CONTRIBUTORS "AS IS" AND ANY
513 EXPRESS OR IMPLIED WARRANTIES, INCLUDING, BUT NOT LIMITED TO, THE IMPLIED WARRANTIES OF
514 MERCHANTABILITY AND FITNESS FOR A PARTICULAR PURPOSE ARE DISCLAIMED. IN NO EVENT SHALL
515 THE COPYRIGHT HOLDER OR CONTRIBUTORS BE LIABLE FOR ANY DIRECT, INDIRECT, INCIDENTAL,
516 SPECIAL, EXEMPLARY, OR CONSEQUENTIAL DAMAGES (INCLUDING, BUT NOT LIMITED TO,
517 PROCUREMENT OF SUBSTITUTE GOODS OR SERVICES; LOSS OF USE, DATA, OR PROFITS; OR BUSINESS
518 INTERRUPTION) HOWEVER CAUSED AND ON ANY THEORY OF LIABILITY, WHETHER IN CONTRACT, STRICT
519 LIABILITY, OR TORT (INCLUDING NEGLIGENCE OR OTHERWISE) ARISING IN ANY WAY OUT OF THE USE OF
520 THIS SOFTWARE, EVEN IF ADVISED OF THE POSSIBILITY OF SUCH DAMAGE.

521 The software includes `errorbarxy.m` by Qi An (2016) (BSD-2-Clause License)
522 (<http://www.mathworks.com/matlabcentral/fileexchange/40221>).

523

524 **9 Author Contributions**

525 K. Iyer and D.W. Schmid developed the code. K. Iyer implemented the code and wrote the manuscript.
526 H. Svensen guided code development and provided input data from field studies. D. W. Schmid and H.
527 Svensen edited the manuscript.

528

529 **10 Competing Interests**

530 The authors declare that they have no conflict of interest.

531

532 **11 Acknowledgements**

533 The authors would like to thank two anonymous reviewers for their constructive reviews which helped
534 us better evaluate the model and manuscript.

535

536 **11.2 References**

537 Aarnes, I., Fristad, K., Planke, S., and Svensen, H.: The impact of host-rock composition on
538 devolatilization of sedimentary rocks during contact metamorphism around mafic sheet intrusions,
539 *Geochim. Geophys. Geosyst.*, 12, Q10019, 2011a.
540 Aarnes, I., Planke, S., Trulsvik, M., and Svensen, H.: Contact metamorphism and thermogenic gas
541 generation in the Vøring and Møre basins, offshore Norway, during the Paleocene–Eocene thermal
542 maximum, *Journal of the Geological Society*, doi: 10.1144/jgs2014-098, 2015. 588-598, 2015.
543 Aarnes, I., Svensen, H., Connolly, J. A. D., and Podladchikov, Y. Y.: How contact metamorphism can
544 trigger global climate changes: Modeling gas generation around igneous sills in sedimentary basins,
545 *Geochimica Et Cosmochimica Acta*, 74, 7179-7195, 2010.
546 Aarnes, I., Svensen, H., Polteau, S., and Planke, S.: Contact metamorphic devolatilization of shales in the
547 Karoo Basin, South Africa, and the effects of multiple sill intrusions, *Chemical Geology*, 281, 181-194,
548 2011b.
549 Archer, S. G., Bergman, S. C., Iliffe, J., Murphy, C. M., and Thornton, M.: Palaeogene igneous rocks reveal
550 new insights into the geodynamic evolution and petroleum potential of the Rockall Trough, NE Atlantic
551 Margin, *Basin Research*, 17, 171-201, 2005.
552 Braun, J., Guillocheau, F., Robin, C., Baby, G., and Jelsma, H.: Rapid erosion of the Southern African
553 Plateau as it climbs over a mantle superswell, *Journal of Geophysical Research: Solid Earth*, 119, 6093-
554 6112, 2014.
555 Catuneanu, O., Hancox, P., and Rubidge, B.: Reciprocal flexural behaviour and contrasting stratigraphies:
556 a new basin development model for the Karoo retroarc foreland system, South Africa, *Basin Research*,
557 10, 417-439, 1998.
558 Chevallier, L. and Woodford, A.: Morpho-tectonics and mechanism of emplacement of the dolerite rings
559 and sills of the western Karoo, South Africa, *S. Afr. J. Geol.*, 102, 43-54, 1999.

Formatted: Heading 1, Line spacing: single

Formatted: Line spacing: Multiple 1.15 li

560 Connolly, J. and Petrini, K.: An automated strategy for calculation of phase diagram sections and
561 retrieval of rock properties as a function of physical conditions, *Journal of Metamorphic Geology*, 20,
562 697-708, 2002.

563 du Toit, A. L.: the Karoo dolerites of south Africa: a study in hypabyssal injection, *S. Afr. J. Geol.*, 23, 1-
564 42, 1920.

565 Duncan, A., Erlank, A., Marsh, J., and Cox, K.: Regional geochemistry of the Karoo igneous province,
566 1984. 1984.

567 Fjeldskaar, W., Helset, H. M., Johansen, H., Grunnaleiten, I., and Horstad, I.: Thermal modelling of
568 magmatic intrusions in the Gjallar Ridge, Norwegian Sea: implications for vitrinite reflectance and
569 hydrocarbon maturation, *Basin Research*, 20, 143-159, 2008.

570 Galushkin, Y. I.: Thermal effects of igneous intrusions on maturity of organic matter: A possible
571 mechanism of intrusion, *Organic Geochemistry*, 26, 645-658, 1997.

572 Hantschel, T. and Kauerauf, A. I.: *Fundamentals of Basin and Petroleum Systems Modeling*, Springer-
573 Verlag Berlin Heidelberg, 2009.

574 Iyer, K., Rüpke, L., and Galerne, C. Y.: Modeling fluid flow in sedimentary basins with sill intrusions:
575 Implications for hydrothermal venting and climate change, *Geochemistry, Geophysics, Geosystems*, 14,
576 5244-5262, 2013.

577 Iyer, K., Schmid, D. W., Planke, S., and Millett, J.: Modelling hydrothermal venting in volcanic
578 sedimentary basins: Impact on hydrocarbon maturation and paleoclimate, *Earth and Planetary Science*
579 *Letters*, 467, 30-42, 2017.

580 Jaeger, J.: Thermal effects of intrusions, *Reviews of Geophysics*, 2, 443-466, 1964.

581 Jaeger, J. C.: The temperature in the neighborhood of a cooling intrusive sheet, *Am J Sci*, 255, 306-318,
582 1957.

583 Jaeger, J. C.: Temperatures outside a cooling intrusive sheet, *Am J Sci*, 257, 44-54, 1959.

584 Jamtveit, B., Bucher-Nurminen, K., and Stijfhoorn, D. E.: Contact Metamorphism of Layered Shale-
585 Carbonate Sequences in the Oslo Rift: I. Buffering, Infiltration, and the Mechanisms of Mass Transport,
586 *Journal of Petrology*, 33, 377-422, 1992.

587 Jamtveit, B., Svensen, H., Podladchikov, Y. Y., and Planke, S.: Hydrothermal vent complexes associated
588 with sill intrusions in sedimentary basins. In: *Physical Geology of High-Level Magmatic Systems*,
589 Breitkreuz, C. and Petford, N. (Eds.), Geological Society Special Publication, Geological Soc Publishing
590 House, Bath, 2004.

591 Kjoberg, S., Schmiedel, T., Planke, S., Svensen, H. H., Millett, J. M., Jerram, D. A., Galland, O., Lecomte, I.,
592 Schofield, N., and Haug, Ø. T.: 3D structure and formation of hydrothermal vent complexes at the
593 Paleocene-Eocene transition, the Møre Basin, mid-Norwegian margin, *Interpretation*, 5, SK65-SK81,
594 2017.

595 Lovering, T.: Theory of heat conduction applied to geological problems, *Geological Society of America*
596 *Bulletin*, 46, 69-94, 1935.

597 Malthe-Sorensen, A., Planke, S., Svensen, H., and Jamtveit, B.: Formation of saucer-shaped sills. In:
598 *Physical Geology of High-Level Magmatic Systems*, Breitkreuz, C. and Petford, N. (Eds.), Geological
599 Society Special Publication, Geological Soc Publishing House, Bath, 2004.

600 Monreal, F. R., Villar, H. J., Baudino, R., Delpino, D., and Zencich, S.: Modeling an atypical petroleum
601 system: A case study of hydrocarbon generation, migration and accumulation related to igneous
602 intrusions in the Neuquen Basin, Argentina, *Marine and Petroleum Geology*, 26, 590-605, 2009.

603 Moorcroft, D. and Tonnelier, N.: Contact Metamorphism of Black Shales in the Thermal Aureole of a
604 Dolerite Sill Within the Karoo Basin. In: *Origin and Evolution of the Cape Mountains and Karoo Basin*,
605 Springer, 2016.

606 Muirhead, D. K., Bowden, S. A., Parnell, J., and Schofield, N.: Source rock maturation owing to igneous
607 intrusion in rifted margin petroleum systems, *Journal of the Geological Society*, doi: 10.1144/jgs2017-
608 011, 2017. 2017.

609 Peace, A., McCaffrey, K., Imber, J., Hobbs, R., van Hunen, J., and Gerdes, K.: Quantifying the influence of
610 sill intrusion on the thermal evolution of organic-rich sedimentary rocks in nonvolcanic passive margins:
611 an example from ODP 210-1276, offshore Newfoundland, Canada, *Basin Research*, 29, 249-265, 2017.

612 Pepper, A. S. and Corvi, P. J.: Simple kinetic models of petroleum formation. Part I: oil and gas
613 generation from kerogen, *Marine and Petroleum Geology*, 12, 291-319, 1995.

614 Planke, S., Rasmussen, T., Rey, S. S., and Myklebust, R.: Seismic characteristics and distribution of
615 volcanic intrusions and hydrothermal vent complexes in the Vøring and Møre basins. In: *Petroleum
616 Geology: North-western Europe and global perspectives - Proceedings of the 6th Petroleum Geology
617 Conference*, Doré, A. G. and Vining, B. A. (Eds.), Geological Society, London, 2005.

618 Svensen, H., Corfu, F., Polteau, S., Hammer, O., and Planke, S.: Rapid magma emplacement in the Karoo
619 Large Igneous Province, *Earth and Planetary Science Letters*, 325, 1-9, 2012.

620 Svensen, H. and Jamtveit, B.: Metamorphic Fluids and Global Environmental Changes, *ELEMENTS*, 6,
621 179-182, 2010.

622 Svensen, H., Planke, S., Chevallier, L., Malthe-Sørensen, A., Corfu, F., and Jamtveit, B.: Hydrothermal
623 venting of greenhouse gases triggering Early Jurassic global warming, *Earth and Planetary Science
624 Letters*, 256, 554-566, 2007.

625 Svensen, H., Planke, S., Malthe-Sørensen, A., Jamtveit, B., Myklebust, R., Rasmussen Eidem, T., and Rey,
626 S. S.: Release of methane from a volcanic basin as a mechanism for initial Eocene global warming,
627 *Nature*, 429, 542-545, 2004.

628 Svensen, H., Planke, S., Polozov, A. G., Schmidbauer, N., Corfu, F., Podladchikov, Y. Y., and Jamtveit, B.:
629 Siberian gas venting and the end-Permian environmental crisis, *Earth and Planetary Science Letters*, 277,
630 490-500, 2009.

631 Svensen, H. H., Planke, S., Neumann, E.-R., Aarnes, I., Marsh, J. S., Polteau, S., Harstad, C. H., and
632 Chevallier, L.: Sub-Volcanic Intrusions and the Link to Global Climatic and Environmental Changes, 2015.
633 2015.

634 Sweeney, J. and Burnham, A. K.: Evaluation of a simple model of vitrinite reflectance based on chemical
635 kinetics, *AAPG Bulletin*, 74, 1559-1570, 1990.

636 Tankard, A., Welsink, H., Aukes, P., Newton, R., and Stettler, E.: Tectonic evolution of the Cape and
637 Karoo basins of South Africa, *Marine and Petroleum Geology*, 26, 1379-1412, 2009.

638 Tracy, R. J. and Frost, B. R.: Phase equilibria and thermobarometry of calcareous, ultramafic and mafic
639 rocks, and iron formations, *Reviews in Mineralogy and Geochemistry*, 26, 207-289, 1991.

640 Walker, F. and Poldervaart, A.: Karoo dolerites of the Union of South Africa, *Geological Society of
641 America Bulletin*, 60, 591-706, 1949.

642 Wang, D.: MagmaHeatNS1D: One-dimensional visualization numerical simulator for computing thermal
643 evolution in a contact metamorphic aureole, *Computers & Geosciences*, 54, 21-27, 2013.

644 Wang, D. and Manga, M.: Organic matter maturation in the contact aureole of an igneous sill as a tracer
645 of hydrothermal convection, *Journal of Geophysical Research: Solid Earth*, 120, 4102-4112, 2015.

646 Wang, D. Y.: Comparable study on the effect of errors and uncertainties of heat transfer models on
647 quantitative evaluation of thermal alteration in contact metamorphic aureoles: Thermophysical
648 parameters, intrusion mechanism, pore-water volatilization and mathematical equations, *International
649 Journal of Coal Geology*, 95, 12-19, 2012.

650 Wang, D. Y., Lu, X. C., Song, Y. C., Shao, R., and Qi, T. A.: Influence of the temperature dependence of
651 thermal parameters of heat conduction models on the reconstruction of thermal history of igneous-
652 intrusion-bearing basins, *Computers & Geosciences*, 36, 1339-1344, 2010.

653 Wang, D. Y. and Song, Y. C.: Influence of different boiling points of pore water around an igneous sill on
654 the thermal evolution of the contact aureole, *International Journal of Coal Geology*, 104, 1-8, 2012.
655 Wang, D. Y., Song, Y. C., Liu, Y., Zhao, M. L., Qi, T., and Liu, W. G.: The influence of igneous intrusions on
656 the peak temperatures of host rocks: Finite-time emplacement, evaporation, dehydration, and
657 decarbonation, *Computers & Geosciences*, 38, 99-106, 2012a.
658 Wang, K., Lu, X. C., Chen, M., Ma, Y. M., Liu, K. Y., Liu, L. Q., Li, X. Z., and Hu, W. X.: Numerical modelling
659 of the hydrocarbon generation of Tertiary source rocks intruded by doleritic sills in the Zhanhua
660 depression, Bohai Bay Basin, China, *Basin Research*, 24, 234-247, 2012b.